On the production and properties of novel particulate $NiTi_p$/AA2124 metal matrix composites

D. San Martín[a*], D.D. Risanti[b,c], G. Garcés[d], P.E.J. Rivera-Diaz-del-Castillo[b], S. van der Zwaag[b]

[a]MATERALIA group, Department of Physical Metallurgy, Centro Nacional de Investigaciones Metalúrgicas (CENIM-CSIC), Av. Gregorio del Amo 8, 28040 Madrid, Spain.

[b]NOVAM group, Faculty of Aerospace Engineering, Delft University of Technology, Kluyverweg 1, 2629 HS, Delft, The Netherlands.

[c]Materials for Innovation Institute (M2i), Mekeweg 2, 2628 CD Delft, The Netherlands.

[d]Department of Physical Metallurgy, Centro Nacional de Investigaciones Metalúrgicas (CENIM-CSIC), Av. Gregorio del Amo 8, 28040 Madrid, Spain.

Abstract: Novel aluminium (AA2124) matrix composites reinforced with 10 and 20 vol.% NiTi particulates have been fabricated by using powder metallurgy processing techniques. It is shown that in the as-extruded condition the composite materials show enhanced damping capacity and improved compressive strength compared to the unreinforced material produced similarly.

Keywords: Composite materials, AA2124, NiTi, martensitic transformation, damping capacity, mechanical properties.

*Corresponding author:

David San Martin,

Department of Physical Metallurgy,

Centro Nacional de Investigaciones Metalúrgicas (CENIM, CSIC),

Av. Gregorio del Amo 8,

28760 Madrid,

Spain.

E-mail: dsm@cenim.csic.es.

Tel. +34915538900 (ext. 285);

Fax: +34915347425.

1. Introduction

Shape memory alloys (SMAs) have attracted much interest due to their ability to recover their original shape after a pseudo-plastic deformation step, causing the so-called shape memory effect (SME) [1]. This unique shape memory behavior is due to a temperature-dependent, martensitic phase transformation within the microstructure of the material. Due to this characteristic property, SMAs have found application as sensors or/and actuators in smart systems. In addition, due to their high damping capacity, these materials are also applied to control vibrations in materials subjected to dynamic loads, substituting hydraulic systems encountered in earthquake shock dampers, and systems to reduce noise in the aerospace industry.

A number of papers appeared in the last decade dealing with the shape recovery of SMA fibers embedded in a polymer or metal matrix. These composites showed a significant strength improvement compared to unreinforced material [2,3]. Only a few examples are found in the literature on the use of SMA particulates instead of SMA fibers [4,5,6]. However, so far these composites have found no practical applicability because of the matrix materials used was pure aluminium or iridium. The challenge is to produce SMA-metal matrix composites (SMA-MMCs) with real potential applicability.

The present work describes the successful fabrication of aluminium (AA2124) matrix composites reinforced with 10 and 20 vol.% NiTi particulates, respectively. Scanning electron microscopy (SEM-EDS), X-ray diffraction, internal friction measurements and mechanical tests have been used to characterize the composites. The microstructure of the composites produced by hot extrusion is free of undesirable intermetallic phases. In addition, it is shown that the reinforcement with NiTi particulates greatly enhances the

damping capacity and improves compressive strength compared to the unreinforced material.

2. Experimental procedures

AA2124-based aluminium alloy composites containing 0, 10 and 20 vol. % NiTi particulates have been manufactured; these materials will be named as 0R, 10R and 20R, respectively. Powder particulates of AA2124, with an average diameter of 32 μm, have been acquired from Alpoco (UK). The composition of the as-received aluminium powders is (wt.%): 3.93Cu-1.41Mg-0.64Mn-0.21Si-0.06Fe. The NiTi particulates, with an average diameter of 30 μm and a nickel fraction of 55.7 wt.%, were purchased from Nanoval GmbH&Co. KG (Germany). After mixing the powders for 10 hours using a Turbula® Powder Blender, the blend was encapsulated in aluminium (AA6063) tubes with an internal diameter of 40 mm. The tubes were kept at 773 K for 900 seconds before cooling down to the extrusion temperature. For materials 0R, 10R and 20R the extrusion temperatures were 703, 713 and 703 K, respectively; while the peak extrusion pressures were 650, 500 and 650 MPa, respectively. The extrusion rate used was 0.4 mm/s. Rods with a diameter 10.4 mm were obtained as a result of the extrusion process.

For the metallographic inspection, some pieces were cut along the extrusion direction, mounted in cold epoxy resin, ground and polished, finishing using a colloidal silica solution. A JEOL JSM-6500 field-emission gun scanning electron microscope (FEG-SEM) equipped with an energy dispersive spectrometer (EDS) was used. Analyses of the phases present in the microstructure have been carried out using a Siemens D5000 X-ray

Diffractometer on the samples prepared for metallographic inspection. Monochromatic CuK_α X-ray radiation, of wavelength λ=0.15406 nm, was used.

To study the damping capacity of the composites, temperature dependent internal friction (TDIF) measurements were carried out using an inverted free torsion pendulum under high vacuum (10^{-5} mbar). The temperature evolution of the frequency was recorded simultaneously. Samples of dimensions (L×W×T=) 58 mm×4 mm×1 mm machined along the extrusion direction have been tested using a constant strain amplitude of 5×10^{-5}, covering a range of temperatures from 100 K up to 325 K and using a heating/cooling rate of 0.033 K/s.

Cylindrical samples of 3 mm in diameter and 10 mm gauge length have been used for the tensile tests, while cylinders of 5 mm in diameter and 8 mm in height have been used for the compression tests. These tests were carried out at room temperature, using a strain rate of $\dot{\varepsilon}=10^{-3}$ s^{-1} and each test was repeated at least twice.

3. Results and discussion

3.1 Microstructure

Figure 1a-b shows characteristic backscattered electron images of the microstructure of composites 10R and 20R. NiTi particulates appear as white quasi-circular phases embedded in the grey aluminium matrix. NiTi particulates are homogeneously distributed in the aluminium matrix. In contrast to a previous attempt to make such composites [7], no intermetallic phases were detected at the interface between NiTi/Al matrix; however, SEM-EDS chemical analyses show that some Al and Cu have diffused into the NiTi particulates.

These elements are homogeneously distributed inside the NiTi particulates, whose composition is very similar in composites 10R and 20R: 51Ni-41Ti-6Al-2Cu (in wt.%). Figure 2 shows the X-ray diffractograms, recorded at room temperature. Peaks corresponding to the following phases have been detected in the microstructure: FCC-Al (α), NiTi (B2), Al_2CuMg (S') and Al_2Cu (θ'). These results confirm that no undesirable intermetallic phases are present in the microstructure of 10R and 20R. Three peaks related to NiTi particulates are observed: (110), (200) and (211) planes of the B2-austenitic phase. As it would be expected, the intensity of NiTi peaks increases while the intensity of precipitate peaks decreases with the amount of reinforcement in the material.

3.2 Damping capacity

Figure 3 shows the TDIF (Q^{-1}) spectrum and frequency. A flat spectrum is observed for sample 0R implying that all damping peaks in the composite samples are due to the presence of the NiTi particulates. The relaxation strength increases with the SMA content. Three peaks are visible on cooling (blue): 1) Peak $P_{A\rightarrow R}$ related to the austenite (B2) to R-phase transformation [8]; 2) peak $P_{R\rightarrow M}$ related to the R-phase to monoclinic martensite (B19') transformation; and 3) peak P_{Rel}. On the other hand, two peaks are visible on heating (red): 1) Peak $P_{M\rightarrow A}$ related to the martensite to austenite transformation and 2) peak P_{Rel}. Peak transformation temperatures as well as the corresponding Q^{-1} (IF) values derived from this figure are given in Table 1. The temperature evolution of the frequency, which is related to the shear modulus of the sample ($f \sim \sqrt{G}$), decreases with increasing temperature, showing a clear minimum for $P_{A\rightarrow R}$ and $P_{M\rightarrow A}$, characteristic of a phase

transformation. Previous literature, suggest that peak P_{Rel} is associated to the thermally activated movement of twin-related dislocations pinned by point defects (vacancies or Ti_3Ni_4) in the martensite or R-phase inside NiTi particulates [9] rather than a process originated at the interface matrix/reinforcement [10].

3.3 Mechanical properties

Figure 4 shows characteristic compression and tension behaviour at room temperature. Only the non-linear part of the stress-strain plots is represented. Moreover, for the tensile curves, only the values up to the ultimate tensile strength (UTS) are shown in this figure. The objective of these experiments was to find out the influence of the reinforcement alone on the mechanical behavior of the composites without accounting for the influence of the SME. The yield stress (YS) and UTS are not influenced significantly by the reinforcement and values around 210-220 and 320-340 MPa, respectively, are obtained for all materials; by contrast, the uniform elongation (UE) drops from around 13%, for sample 0R, to around 6-7% for the reinforced materials. The SMA-MMCs show very poor ductility, breaking at the UTS without necking, while 0R samples show significant elongation beyond the UTS, reaching a true fracture strain of around 65%. On the other hand, under compressive loading there is a significant strain hardening up to plastic strain levels of 0.04-0.05 in sample 20R compared to sample 0R. As a result, the compressive strength increases significantly (10-15%) for strain levels above 0.05. For sample 10R, this effect is weaker.

4. Conclusions

Novel aluminium (AA2124) matrix composites reinforced with 10 and 20 vol.% NiTi particulates have been fabricated. No intermetallic phases have been observed at the interface NiTi/Al. The composite materials show enhanced damping capacity at low temperatures and improved compressive strength compared to the unreinforced material. The yield stress (YS) and the ultimate tensile strength (UTS) are comparable with respect to the unreinforced material, although the uniform elongation is decreased.

5. Acknowledgements

We are thankful to MicroNed Research Program (workpackage 1-C-4) and the Materials Innovation Institute (M2i) in The Netherlands for the financial support. Mr. Javier Vara Miñambres, Mr. Nacho Ruiz Oliva and Mr. Cesar Moreno from CENIM (Spain) are thanked for the experimental support.

6. References

[1] K. Otsuka, X. Ren, Intermetallics 7 (1999) 511-528.

[2] A. Shimamoto, H. Ohkawara, F. Nogata, Eng. Fract. Mech. 71 (2004) 737–746.

[3] W.D. Armstrong, T. Lorentzen, P. Bréndsted, P.H. Larsen, Acta Mater. 46 (1998) 3455-3466.

[4] J. San Juan, M.L. Nó, Mater. Sci. Eng. A442 (2006) 429-432.

[5] G.A. Porter, P.K. Liaw, T.N. Tiegs and K.H. Wu, Mater. Sci. Eng. A314 (2001) 186-193.

[6] Z.G. Wei, C.Y. Tang, W.B. Lee, L.S. Cui, D.Z. Tang, Mater. Lett. 32 (1997) 313-317.

[7] R.R. Thorat, D.D. Risanti, D. San Martín, G. Garcés, P.E.J. Rivera Díaz del Castillo, S. van der Zwaag, J. Alloys Compd. 477 (2009) 307-315.

[8] T. Kurita, H. Matsumoto, K. Sakamoto, K. Tanji, H. Abe, J. Alloys Compd. 396 (2005) 193-196.

[9] S.-K. Wu, H.-C. Lin, T.-S. Chou, Mater. Trans. 47 (2006) 711-715.

[10] L. Parrini, R. Schaller, Acta Mater. 44 (1996) 4881-4888.

Figure Captions

Figure 1. Backscatter electron image of composites a) 10R and b) 20R

Figure 2. X-ray diffraction patterns for samples 0R (green), 10R (blue) and 20R (red).

Figure 3. Temperature dependent internal friction (TDIF) spectrum and frequency for samples 0R (×), 10R (△) and 20R (O), on cooling (blue) and heating (red) at 2 K/min.

Figure 4. Compression and tension engineering stress-engineering strain curves for samples 0R, 10R and 20R. Strain rate: 10^{-3} s^{-1}.

Figure 1

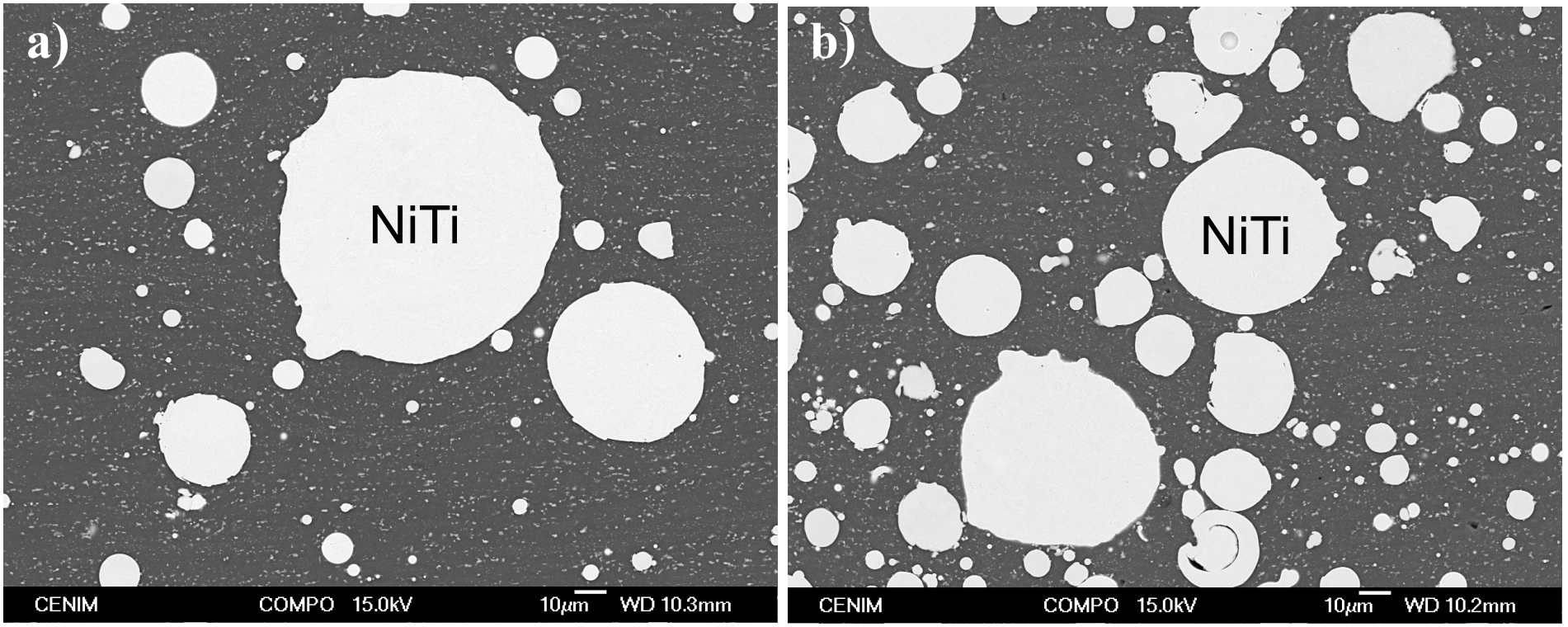
a)
NiTi
CENIM COMPO 15.0kV 10μm WD 10.3mm
b)
NiTi
CENIM COMPO 15.0kV 10μm WD 10.2mm

Figure 2 - Color

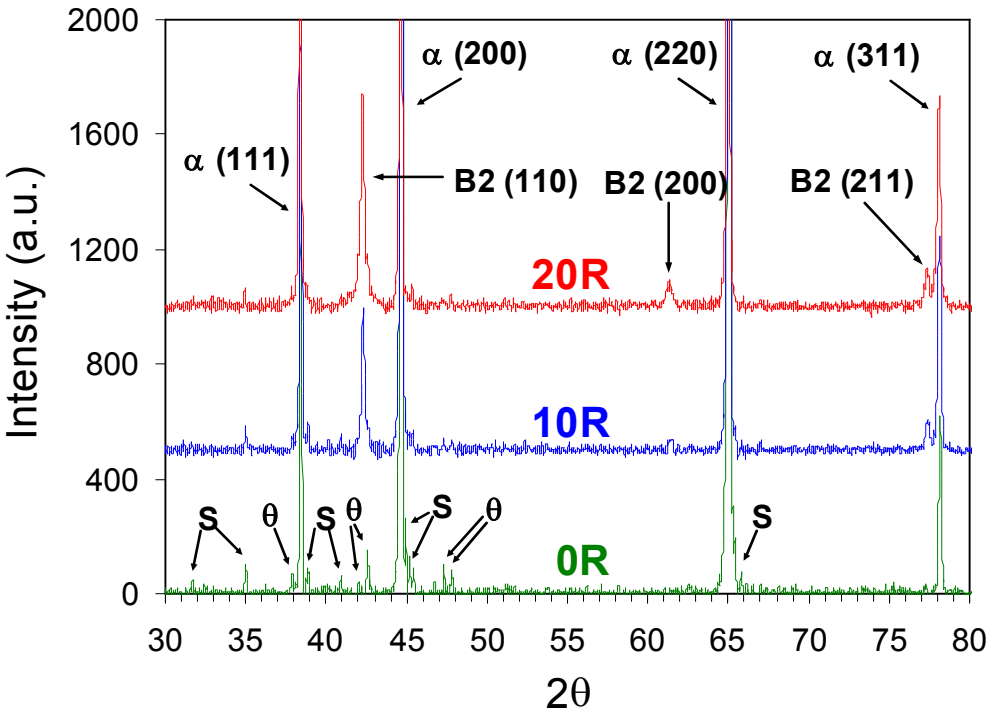

Figure 3 - Color

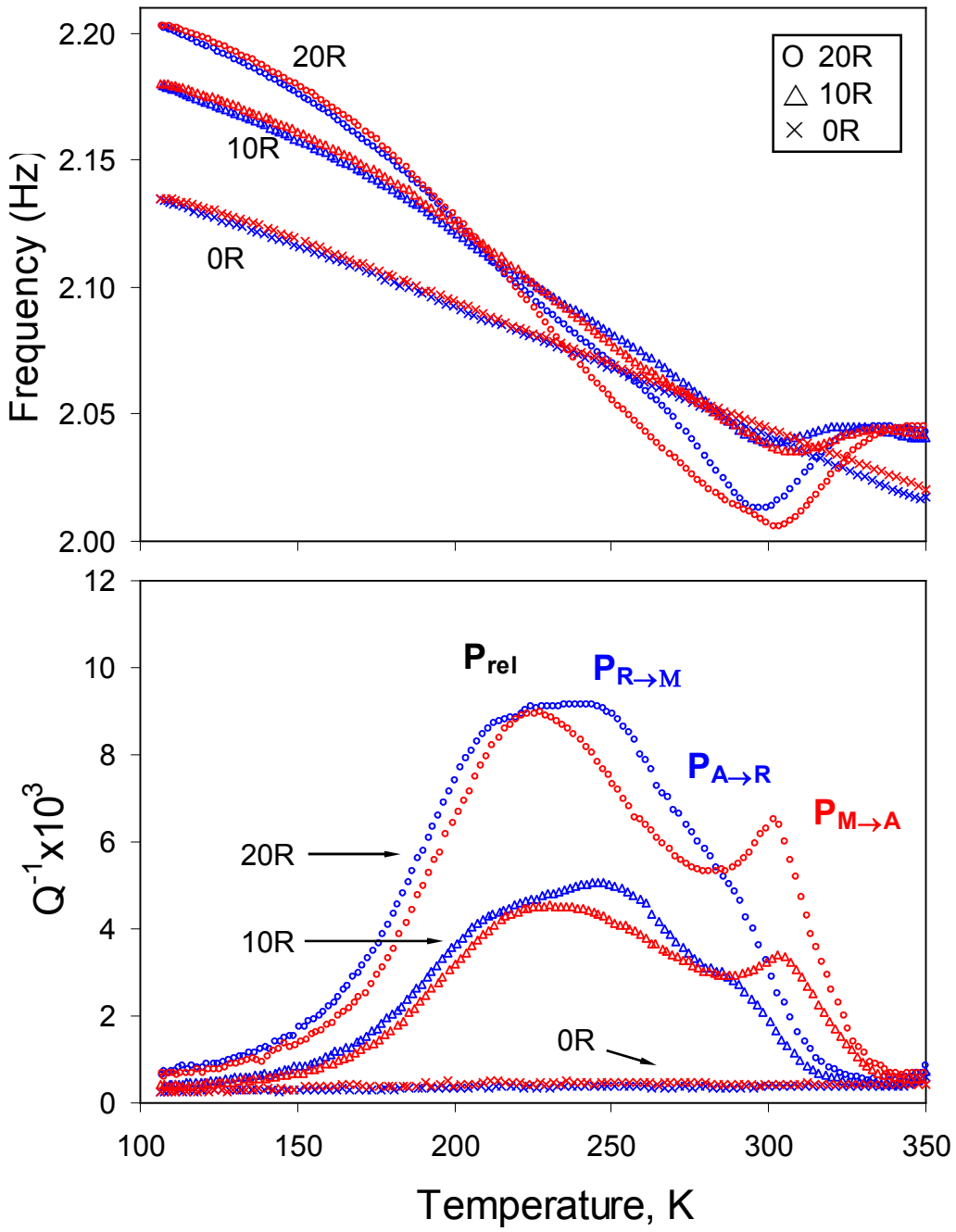

Figure 4 - Color

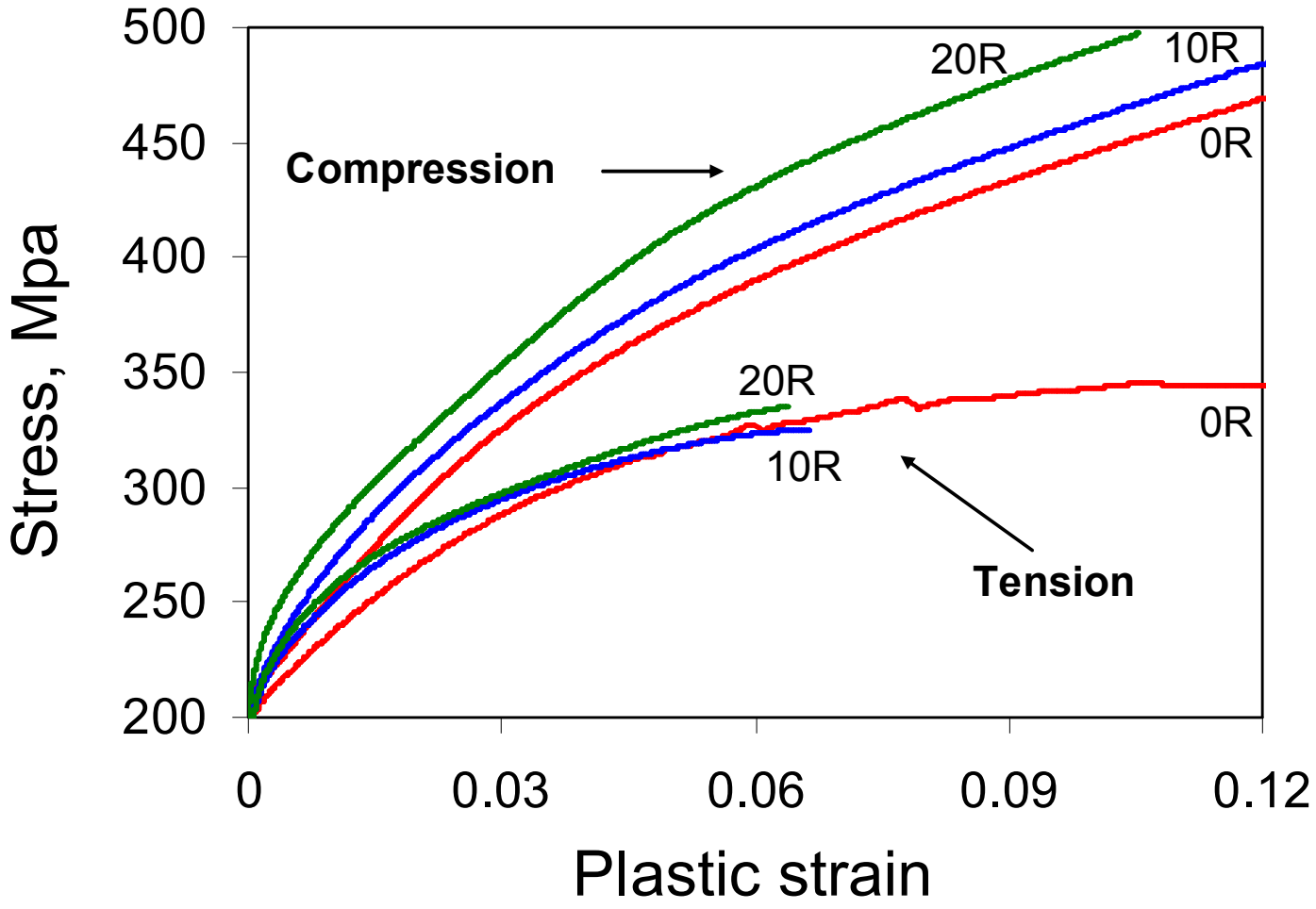

Table 1

Table 1. Peak transition temperatures and their corresponding internal friction values (IF), evaluated from Figure 3. For the determination of the peak internal friction values, the results for samples 0R have been consider as the offset.

	$P_{A\rightarrow R}$		$P_{R\rightarrow M}$		P_{Rel} (cooling)		P_{Rel} (heating)		$P_{M\rightarrow A}$	
	T, K	IF, $\times 10^{-3}$	T, K	IF, $\times 10^{-3}$	T, K	IF, $\times 10^{-3}$	T, K	IF, $\times 10^{-3}$	T, K	IF, $\times 10^{-3}$
10R	284	2.5	246	4.7	216	4.0	231	4.1	302	3.0
20R	289	4.5	240	8.8	217	8.5	229	8.5	302	6.1